RESEARCH ARTICLE

A Wideband High-Gain Circularly-Polarized Dielectric Horn Antenna Equipped With Lamé-Axicon Stacked-Disk Lens for Remote Sensing, Air Traffic Control and Satellite Communications

DIEGO CARATELLI[1,2], (Senior Member, IEEE),
RENATO CICCHETTI[3], (Life Senior Member, IEEE), VALENTINA CICCHETTI[3],
AND ORLANDINO TESTA[3]

[1]Department of Research and Development, The Antenna Company, 5656 AE Eindhoven, The Netherlands
[2]Department of Electrical Engineering, Eindhoven University of Technology, 5612 AP Eindhoven, The Netherlands
[3]Department of Information Engineering, Electronics and Telecommunications, University of Rome "La Sapienza," 00184 Rome, Italy

Corresponding author: Renato Cicchetti (renato.cicchetti@uniroma1.it)

ABSTRACT A wideband high-gain circularly polarized (CP) shaped dielectric horn-lens antenna (SDHLA) operating in the frequency band between 6.7 and 18.2 GHz [fractional impedance bandwidth (FIBW) of 92.4%] with a 3-dB axial-ratio in the frequency range from 8.1 to 16.3 GHz [fractional axial-ratio bandwidth (FARBW) of 67.2%], is presented. The antenna, composed of a suitably shaped dielectric horn, integrated with a super-ellipsoidal-axicon dielectric lens made out of stacked thin dielectric disks, is mounted on a printed circuit board (PCB) where a microstrip line terminated with a wideband radial stub is used to excite a S-shaped slot through which the circular polarization is achieved. Parameterized 3D Lamé curves, describing the horn and lens profile, are used to optimize the antenna design. The antenna features a peak realized gain exceeding 13.1 dBi that is beneficial in a variety of applications, such as digital video broadcasting (DVB), remote sensing, weather monitoring, satellite communications, and air traffic control. The full-wave electromagnetic solver CST Studio Suite™, based on a locally conformal finite integration technique (FIT), was employed to design and characterize the antenna whose performances were found to be in good agreement with the experimental measurements.

INDEX TERMS Broadband excitation slot, circular polarization, dielectric lens, dielectric horn, dielectric resonator antennas (DRAs), satellite communications, super-ellipsoidal–axicon dielectric lens, stacked-disk dielectric lens, ultrawideband (UWB), wideband antennas, wireless communications.

I. INTRODUCTION

Circularly polarized (CP) radio communication systems are preferable over the linearly polarized counterparts when insensitivity to the relative orientation between transceivers (orientation-independent characteristics), greater robustness to multipath effects [1] as well as to the propagation

The associate editor coordinating the review of this manuscript and approving it for publication was Wei E. I. Sha.

characteristics of the radio channel in presence of hydrometeors, clouds, fog, and plasma, which typically affect satellite radio links [2], are required. In addition to polarization requirements, modern communication systems must guarantee high gain and wide bandwidth when high data rates must be ensured in point-to-point (indoor/outdoor), short-, long-range or satellite communication links [2], [3], [4]. In this context, high-gain circularly polarized wideband dielectric resonator antennas (DRAs) can result particularly effective.

Indeed, DRAs have several attractive characteristics, such as no surface wave losses, high radiation efficiency, compact size, nearly constant gain, high impedance bandwidth, and flexibility in exciting linear/circular polarization. Furthermore, being basically three-dimensional (3D) radiating structures, they offer additional degrees of freedom to antenna designers.

In DRAs, the CP can be achieved in different ways, through the excitation of degenerate modes [5], [6], the use of dual/four-point electric probes [7], [8], or by probes connected by means of microstrip lines [9], [10], through traveling wave exciters [11], [12], suitable slots [13], [14], by using an appropriate shaping of the ground plane [15], by adding parasitic elements [16], [17], or coupled resonators [18], [19], just to mention some of the main design strategies.

Despite the various techniques used to excite the CP, most DRAs exhibit limited gain and/or operating band which may result incompatible with modern point-to-point terrestrial and satellite communication system requirements [2], [20]. Design efforts aimed at enhancing the performance of DRAs in terms of gain, bandwidth, and polarization purity are proved by the growing number of papers appearing in the technical literature [21], [22], among which those described above stand out. In particular, a moderate-gain broadband parallelepipedal DRA fed by means of a H-shaped metal strip attached to one of its faces in such a way as to excite the relevant degenerate modes $TE^x_{\delta 13}$ and $TE^y_{1\delta 3}$ has been presented in [6]. The proposed antenna exhibits a fractional impedance bandwidth (FIBW) of about 27.7% (3.67-4.73 GHz), a fractional axial-ratio bandwidth (FARBW) of approximately 20% (3.67-4.4 GHz), and a peak realized gain of about 6.8 dBi.

A DRA with FIBW=104.96% (5.70–18.29 GHz) and FARBW=40% (6.6–9.7 GHz), having a maximum gain of 8.41 dBi has been proposed in [10]. Such antenna, that is optimized for aerial applications in C, X, and Ku bands, is composed of a cross-shaped two-layer dielectric resonator (DR) placed inside a dual-cylindrical cavity integrated with a radome. To excite the antenna, two strip probes placed on adjacent faces of the DRA and electrically connected to each other by a semicircular microstrip transmission line were used.

A rectangular DRA excited by an Archimedean spiral slot useful to excite the CP was proposed in [12]. To enable the propagation of a traveling wave in the slot, while suppressing spurious reflections at its termination, a chip resistor was employed. In this way, an impedance band ranging from 1.8 to 2.6 GHz (FIBW=36.36%) was achieved in combination with an AR bandwidth of 25.7% (1.93–2.50 GHz). The proposed antenna delivers an average gain of about 4.52 dBi within the axial-ratio band.

A first example of high-gain wideband DRA using a dielectric spherical-axicon lens and a metal reflector was presented in [8]. The proposed antenna, operating in the frequency range from 4.6 to 9.1 GHz (FIBW=65%) with a peak gain exceeding 14 dBi, can support linear or circular polarization thanks to the adoption of four electric probes,

suitably excited, attached to the external wall of a hollow CDRA on the top of which the spherical-axicon dielectric lens is mounted.

In this paper, a single-feed wideband circularly polarized high-gain shaped-dielectric-horn-lens antenna (SDHLA) operating in the frequency range between 6.7 and 18.2 GHz (FIBW=92.4%), with a peak realized gain of 13.1 dBi, and with a 3-dB axial-ratio band from 8.1 up to 16.3 GHz (FARBW=67.2%), is presented. The antenna, composed of a suitably shaped dielectric horn, is integrated with a lightweight super-ellipsoidal-axicon dielectric lens made out of simple stacked dielectric disks, whose purpose is to increase the gain, as well as the impedance and axial-ratio bandwidths. The proposed radiating structure is mounted on a PCB where a suitable wideband S-shaped slot coupled to a microstrip line terminated with a radial stub, excites the circular polarization. 3D Lamé equations are used to identify the optimal profiles of the dielectric lens and horn that enable the best antenna performance. In this context, the Lamé equation was chosen as it allows synthesizing a vast class of geometrical shapes by acting on a few simple parameters [23]. The proposed antenna covers the entire X-band and most of the Ku-band, that is useful in several (civil and military) applications, such as radar, digital video broadcasting (DVB), remote sensing, weather monitoring, satellite communications, and air traffic control.

This article is organized into five sections. In Section II, the antenna geometry is illustrated. The antenna design is detailed in Section III, while the related electromagnetic performance is presented and discussed in Section IV. Finally, concluding remarks are summarized in Section V.

II. ANTENNA GEOMETRY

A 3D view of the proposed antenna is shown in Fig. 1a, whereas the relevant 2D cross section in the yz-plane is illustrated in Fig. 1b.

The antenna consists of a dielectric horn integrated with a lens composed of five thin dielectric disks stacked along the lens optical axis (see Fig. 1). The radiating structure is placed on a PCB and excited through an S-shaped slot coupled with a tapered microstrip line terminated with a wideband radial stub (see Fig. 2).

The S-slot is used to excite a left-hand circularly polarized electromagnetic field (LHCP). The dielectric horn transfers the RF energy from the excitation slot region to a suitably shaped lightweight dielectric lens, whose purpose is to enhance the realized gain while keeping the antenna weight limited. To reduce weight and manufacturing complexity, a stacked-disk dielectric lens has been adopted in place of the massive counterpart as it exhibits similar electromagnetic field focusing capability but in combination with an extremely lower weight [24]. These features can be exploited in avionics and satellite applications where weight and manufacturing costs are key requirements.

A tapered microstrip line (characteristic impedance $Z_c = 50\,\Omega$), printed on a Rogers RT5870 substrate (thickness
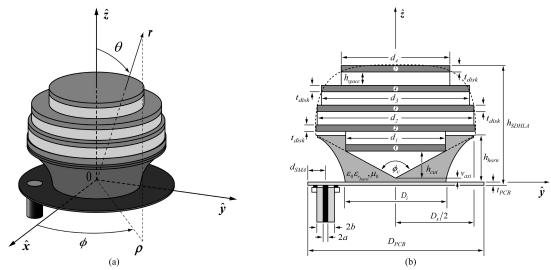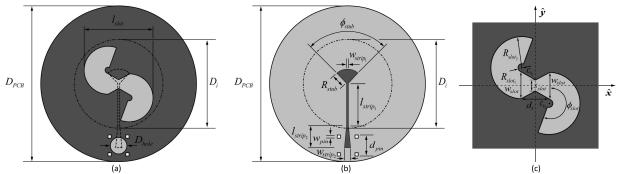
FIGURE 1. Geometry of the shaped-horn-lens antenna. (a) 3-D view and (b) cross-sectional view in the yz-plane. Circled numbers indicate the dielectric disks that make up the 5-stacked-disk dielectric lens. The dashed line in (b) outlines the profile of the reference massive lens. The reference system adopted in the antenna analysis is also shown.

FIGURE 2. Top (a) and bottom (b) views of the PCB hosting the antenna feed structure, and close-up details of the S-shaped excitation slot (c). The dashed circle of diameter D_i in (a) corresponds to the dielectric horn base. A metal void of diameter D_{hole} is realized on the ground plane to compensate for the reactive effects introduced by the microstrip-connector discontinuity. Dark gray metal, light gray dielectric substrate.

$t_{pcb} = 0.787\,mm$, relative permittivity $\varepsilon_{r_{pcb}} = 2.33$, and loss tangent $\tan\delta = 0.0012$), is connected to a surface-mount SMA connector used to feed the antenna. The dielectric horn hosting the lens is made out of Premix low-weight plastic material (relative permittivity $\varepsilon_{r_{horn}} = 3.5$, loss tangent $\tan\delta = 0.0005$), while the five disks forming the lens, each of them having thickness $t_{disk} = 1.524\,mm$, are made out of Rogers TMM4 (relative permittivity $\varepsilon_{r_{disk}} = 4.5$, loss tangent $\tan\delta = 0.0020$). Even if, as suggested in [24], the required separation between the disks forming the lens may be achieved by means of a thin dielectric rod (see [24]), for construction simplicity lightweight disks composed, of a dielectric foam (Styrodur® 3000 CS by Weston) having a thickness $h_{space} = 0.348\,cm$ and relative permittivity $\varepsilon_{r_{spacer}} = 1.05$, were employed as spacers (see Fig. 1b). All the materials used for the antenna manufacturing are inexpensive and easy to find on the market. This allows for the use of the proposed antenna in real-life practical applications.

The parameters describing the optimal geometry of the dielectric horn-lens structure as well as the underlying PCB are reported in Tables 1 and 2, respectively.
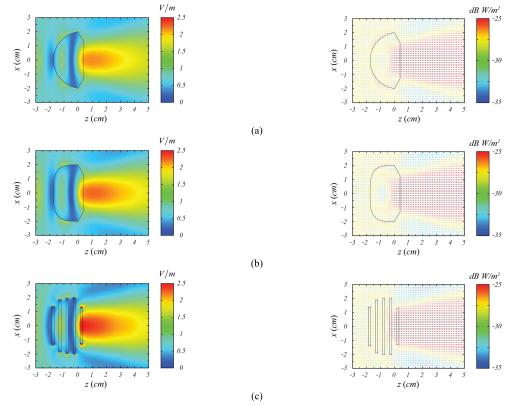
III. ANTENNA DESIGN

The antenna design required the sizing of the dielectric horn and lens, as well as of the PCB on which the horn-lens assembly is housed. Two design steps were necessary to size the dielectric horn. At first, the optimal geometrical parameters of a cylindrical dielectric resonator antenna (CDRA) (diameter $D_i = 2.56\,cm$ and height $h_{horn} = 1.5\,cm$) were evaluated using the empirical formulas reported in [25] so as to ensure the excitation of the $HE_{11\delta}$ resonant mode at the working frequency f = 6 GHz. Then, as suggested in [26], the height of the CDRA was kept constant, while the radiating mouth diameter was widened so to realize a truncated cone structure, which, as observed in [26], allows for a significant broadening of the operating band. The optimal diameter D_s is such to enable the maximum field intensity level received in the slot region when the dielectric horn is excited by a LHCP uniform polarized plane wave normally impinging on it [27].

After completing the horn design, a massive spherical-axicon dielectric lens was preliminarily sized to further increase the field strength in the slot region. After optimization, a dielectric lens having relative permittivity $\varepsilon_{r_{lens}} = 2.1$ (teflon, $\tan\delta = 0.0002$), spherical cap radius $R_{lens} = 2.02\,cm$

FIGURE 3. Geometry of the antenna equipped with (a) the spherical-axicon lens, and (b) the Lamé-axicon lens. The local cylindrical reference system used to describe their geometries is shown in the figure. The region below the dotted line indicates the portion of the axicon lens removed to increase the antenna axial ratio bandwidth.

FIGURE 4. Spatial behavior of the x-component of the electric field and of the real part of the Poynting vector in the xz-plane for (a) massive truncated spherical-axicon lens, (b) truncated massive Lamé-axicon lens, (c) 5-disk lens whose envelope coincides with that of the truncated massive Lamé-axicon lens, excited by an x-polarized uniform plane wave of amplitude $1 V/m$ and frequency f=8 GHz ($D_{lens}/\lambda_0 = 1.07$), traveling along the z-axis. Higher field levels are excited in the back region of the 5-disk lens.

and curvature center in $z_c = -0.27\,cm$ (see Fig. 3), axicon height $h_{axicon} = 1.1\,cm$ and aperture angle $\phi_c = 122°$, has been identified.
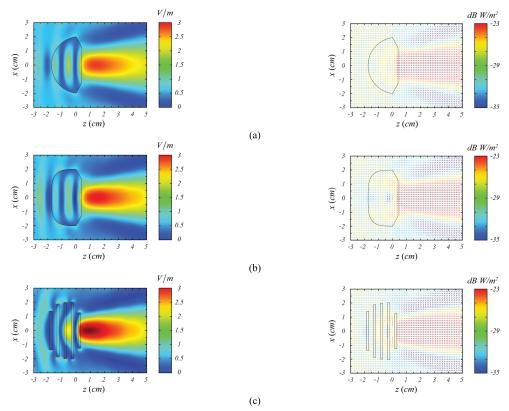
An S-shaped slot etched into the ground plane of the PCB was used to excite a LHCP radiated field in the band of interest. The slot consists of a linearly tapered section followed by a slot having width w_{slot} and circular profile that evolves upwards on one end and downwards on the other end (see Fig. 2), thus resulting in an S-shaped region. The excitation of the antenna was preliminarily modeled using a discrete voltage generator of unitary amplitude placed across the narrow gap of the slot tapered region. The optimization

was carried out by maximizing the antenna gain, impedance, and axial-ratio bandwidths, simultaneously.

Finally, to further increase the antenna gain, lens and horn profile were enhanced using 3D Lamé equations. The following 3D Lamé equation in cylindrical coordinates was used to optimize the lens profile:

$$\left[\frac{\rho}{\sqrt{\left(\frac{D_s}{2}\right)^2 + z_c^2}} \right]^{n_\rho} + \left| \frac{z_{lens} - z_c}{z_{u/l} - z_c} \right|^{n_z} = 1 \forall \rho \in \left[0, \frac{D_s}{2} \right] \tag{1}$$

FIGURE 5. Spatial behavior of the x-component of the electric field and of the real part of the Poynting vector in the xz-plane for (a) massive truncated spherical-axicon lens, (b) truncated massive Lamé-axicon lens, (c) 5-disk lens whose envelope coincides with that of the truncated massive Lamé-axicon lens, excited by an x-polarized uniform plane wave of amplitude 1 V/m and frequency f=12 GHz ($D_{lens}/\lambda_0 = 1.60$), traveling along the z-axis. Higher field levels are excited in the back region of the 5-disk lens.
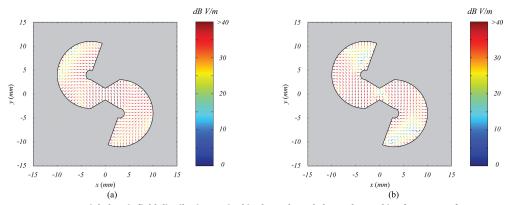

FIGURE 6. Tangential electric field distribution excited in the S-shaped slot at the working frequency of 12 GHz: (a) real part, (b) imaginary part. Spatially and temporally orthogonal field distributions, (responsible for the excitation of the LHCP) are observable in the upper and lower arms of the S-shaped slot. Microstrip excitation level: 1V.

where ρ is the radial cylindrical coordinate (see Fig. 1), while z_u and z_l identify, respectively, the upper and lower limits within which the lens is confined in the local cylindrical reference system (ρ, ϕ, z_{lens}) shown in Fig. 3, while z_c denotes a suitable offset parameter. The spherical-axicon dielectric lens dimensioned in the previous design step is obtained by setting in (1) $n_\rho = n_z = 2$ and $z_c = -0.27\,cm$ for the spherical-cap, and $z_c = 0$ for the axicon lens. To further increase the radiative performance of the antenna, a non-conventional lens geometry [23], [28] was adopted, while

keeping the same vertical bulk. After numerical optimization, the best-performing lens was found to feature an upper profile described by the Lamé parameters $n_\rho = 3.5$, $n_z = 3.5$, $z_c = 0$, with the lower part still coinciding with the axicon introduced during the previous design step.

A similar procedure was carried out to optimize the dielectric horn profile and, in this way, increase the antenna directivity. To this end, the following 3D Lamé equation was used

$$\left|\frac{\rho - \rho_0}{a}\right|^{n_h} + \left|\frac{z_{lens}}{b}\right|^{n_h} = 1 \quad \begin{matrix} \rho_0 \le \rho \le \rho_0 + a \\ b \le z_{lens} \le 0 \end{matrix} \quad (2)$$

TABLE 1. Antenna geometrical parameters.

D_i	2.56 cm
h_{horn}	1.20 cm
D_s	3.94 cm
D_l	4.00 cm
h_{space}	0.348 cm
d_1	2.54 cm
d_2	3.97 cm
d_3	3.76 cm
d_4	2.76 cm
t_{disk}	1.52 mm
d_{disk_1}	2.54 cm
d_{disk_2}	3.97 cm
d_{disk_3}	3.97 cm
d_{disk_4}	3.76 cm
d_{disk_5}	2.76 cm
ϕ_c	122.39°
h_{cut}	0.703 cm
D_{PCB}	4.5 cm
t_{pcb}	0.79 mm
d_{SMA}	0.468 cm
h_{SDHLA}	2.95 cm
v_{axi}	0.1 cm
a	0.064 cm
b	0.215 cm

TABLE 2. Slot and PCB geometrical parameters.

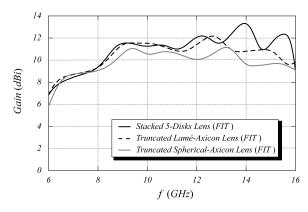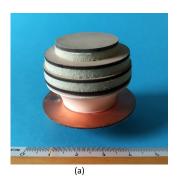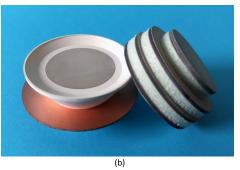|	
s_{slot}	1.2 mm
w_{slot}	6.0 mm
ϕ_{slot}	200°
l_{slot}	20.0 mm
x_{s_1}	-3.0 mm
y_{s_1}	4.0 mm
x_{s_2}	3.0 mm
y_{s_2}	-4.0 mm
R_{slot_1}	1.0 mm
R_{slot_2}	7.0 mm
d_l	6.0 mm
D_{pcb}	45.0 mm
w_{strip_1}	0.5 mm
w_{strip_2}	1.8 mm
l_{strip_1}	12.0 mm
l_{strip_2}	6.5 mm
w_{pin}	1.02 mm
d_{pin}	6.1 mm
R_{stub}	4.15 mm
ϕ_{stub}	83.12°
D_{hole}	5.0 mm

FIGURE 7. Frequency behavior of the realized gain of the shaped dielectric horn stacked-disk lens antenna. A best performance is achieved by the DRA equipped with the stacked 5-disk dielectric lens.

with

$$a = \frac{D_s - D_i}{2} \quad (3)$$

$$b = -h_{horn} \quad (4)$$

$$\rho_0 = \frac{D_i}{2}. \quad (5)$$

After numerical optimization, carried out keeping unchanged the parameters that identify height and horn diameter, as well as those describing the massive lens, an optimal parameter $n_h = 0.7$ was found. Even if the resulting antenna exhibits high realized gain, the axial ratio bandwidth was found not to be suitable for guaranteeing the CP in the band of interest. A significant increase of the axial ratio bandwidth, without affecting the antenna gain, was achieved by removing about the 60% of the axicon lens (see Fig. 3).

Finally, a stacked-disk dielectric lens with the same envelope as the massive counterpart was introduced. Such lens, designed according to the formulas reported in [24], is composed of five dielectric disks having thickness $t_{disk} = 1.524 \, mm$ and relative permittivity $\varepsilon_{r_{disk}} = 4.5$ (Rogers TMM4), equally spaced along the lens axis with a spacing $h_{space} = 0.348 \, cm$ (see Fig. 1). The disk lens is therefore characterized by an effective relative permittivity $\varepsilon_{r_{eff}} = 2.1$

(that is equivalent to that of the massive lens) with a stop-band frequency of about $f_c = 17 \, GHz$, beyond which the lens loses its focusing properties [24].

As it appears from Figs. 4 and 5, the electric field and Poynting vector maps show an improved focusing capability of the stacked-disk lens as compared to the corresponding truncated spherical-axicon and Lamé-axicon lenses, when said lenses are excited by a unit-amplitude uniform plane wave (lenses working in receive mode). Larger field levels are observed in the back region of the stacked-disk dielectric
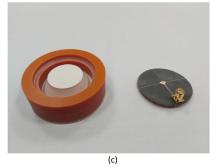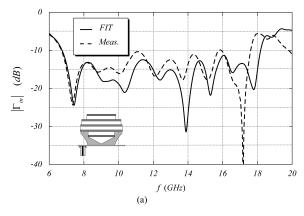
FIGURE 8. Prototype of the SDHLA (a), and detail of the horn and of the 5-stacked-disk dielectric lens assembly (b), mold used for accurate mounting the horn on the PCB (c). The photo in (c) shows the horn inside the mold ready to be glued with the PCB.

TABLE 3. Antenna impedance and axial ratio bandwidth characteristics.

Impedance BW (FIT)	Impedance BW (Meas.)	Axial Ratio BW (FIT)	Axial Ratio BW (Meas.)
f_{min} = 6.7 GHz	f_{min} = 6.7 GHz	f_{min} = 8.1 GHz	f_{min} = 7.8 GHz
f_{max} = 18.2 GHz	f_{max} = 17.6 GHz	f_{max} = 16.3 GHz	f_{max} = 15.8 GHz
FIBW= 92.4%	FIBW= 89.7%	FARBW= 67.2 %	FARBW= 67.8%

TABLE 4. LHCP and RHCP realized gains along the antenna boresight direction.

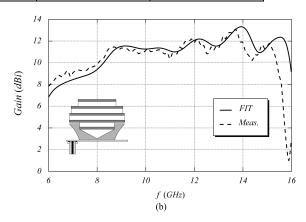| Frequency (GHz)	LHCP Gain (FIT)	LHCP Gain (Meas.)	RHCP Gain (FIT)	RHCP Gain (Meas.)
8	9.4 dBi	9.8 dBi	-4.6 dBi	-8.4 dBi
10	11.3 dBi	11.1 dBi	-18.4 dBi	-13.1 dBi
12	11.9 dBi	11.8 dBi	-13.0 dBi	-6.5 dBi
14	13.3 dBi	11.8 dBi	-12.0 dBi	-5.3 dBi

FIGURE 9. Frequency behavior (a) of the input reflection coefficient magnitude and (b) of the realized gain achieved by the shaped dielectric horn stacked-disk lens antenna. A good agreement between numerical and experimental results can be observed.

lens, thus promoting a higher coupling with the feeding line placed below the S-shaped slot (see Fig. 6). It is worth noting that, although the lenses exhibit free-space normalized dimensions $D_s/\lambda_0 = 1.07$ and $D_s/\lambda_0 = 1.6$ (that are far from those of truly optical lenses) at the frequencies of 8 and 12 GHz, respectively, the achieved focusing effect is anyway significant (see, also, Fig. 12). Finally, for completeness, the frequency behavior of realized gain achieved by the antenna equipped with the three considered dielectric lenses

is reported in Fig. 7. Consistently with the field maps shown in Fig. 4 and 5, the gain performances are better for the antenna equipped with the stacked disk dielectric lens.

Notice that, while the massive lens has a weight equal to 50 g, the one with stacked disks has a weight of only 14 g (equal to 28% of the weight of the massive lens) even though the same realized gain level is achieved. These remarkable characteristics confirm the fact that a stacked-disk lens reduces manufacturing cost and complexity and, therefore,

TABLE 5. Comparison between the performance of the proposed antenna with those available in the literature.

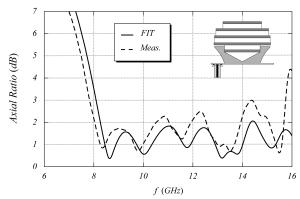| Reference	Excitation Technique	Design Technique	Impedance Bandwidth (GHz)	FIBW (%)	FARBW (%)	Max Gain (dBi)	λ_{max} (mm)	Size Normalized to λ_{max}
[5]	H-Shaped Metal Strip	Parallelepiped DRA	3.67-4.73	27.7	20	6.8	81.69	4.28 x 4.28 x 0.32
[6]	4 Crossing Slots+Microtrip Line	Parallelepiped DRA	1.7-3	55	43.5	8.4	176.35	0.40 x 0.40 x 0.23
[7]	Electric Probes	Shaped DRA	6.7-14	71	71	10	44.75	3.46 x 3.46 x 0.67
[8]	Electric Probes	CDRA+Lens+Reflector	4.6-9.1	65.7	65.7	16	65.17	1.69 x 1.69 x 0.74
[10]	Probes+Conformal Microstrips	Cross-Shaped DRA+Cavity	5.16-17.58	110	32.1	10.8	58.4	1.30 x 1.30 x 0.45
[11]	Resistively Loaded Spiral-Slot	Parallelepiped DRA	1.94–3.24	50	19.2	5.1	154.53	0.32 x 0.32 x 0.075
[12]	Rectangular Spiral Slot	Parallelepiped DRA	1.8-2.6	36.36	25.7	4.95	166.55	0.45 x 0.45 x 0.06
[13]	Cross-Ring Slot	Partially Truncated Parallelepiped DRA	3.02-3.83	24	18.7	5.57	99.26	0.46 x 0.46 x 0.24
[14]	Orthogonal Slots	CDRA	5.5-6.31	13.7	8	5.6	54.51	2.38 x 2.38 x 0.13
[15]	Logarithmic Spiral Slot	CDRA	2.33-2.54	8.6	8.3	1.3	128.67	0.24 x 0.24 x 0.17
[16]	Microstrip Line	Parallelepiped DRA+Parasitic Patch	2.19-2.27	3.6	1.1	3.3	136.89	0.4 x 0.4 x 0.05
[17]	Anular Slot+Parasitic Patch	CDRA	4.25-5.375	23	2.2	4.1	70.54	N.P. x N.P. x 0.17
[18]	Slot	Coupled Parallelepiped DRA	4.9-7	35.3	24.21	5.3	61.18	0.22 x 0.22 x 0.17
[19]	Slot	Coupled Parallelepiped DRA	10.1–13	25.1	19.4	7	29.68	0.77 x 0.77 x 0.2
Proposed SDHLA	S-Shaped Slot	Shaped-Horn-Lens Antenna	6.7-18.2	92.4	67.2	13.1	44.75	1 x 1 x 0.66

FIGURE 10. Frequency behavior of the antenna axis ratio. The differences between measurements and numerical results are probably due to the small misalignments between the different parts forming the antenna as well as to the glue used for its assembly.
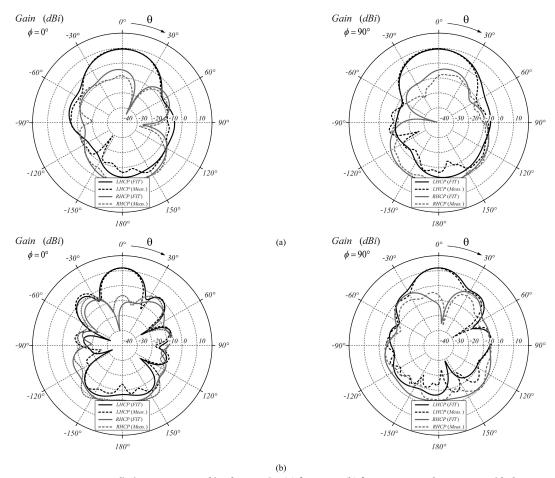
is more suitable in those applications where weight is a key requirement, such as avionics and satellite applications [24].

To guarantee the best performances in terms of impedance bandwidth and axial ratio, a final tuning of the horn height and slot geometry (see Table 1 and 2) was performed. The excitation of the LHCP sustained by the antenna is easily recognizable by the electric field map excited in the S-slot at the frequency of 12 GHz (see Fig. 6).
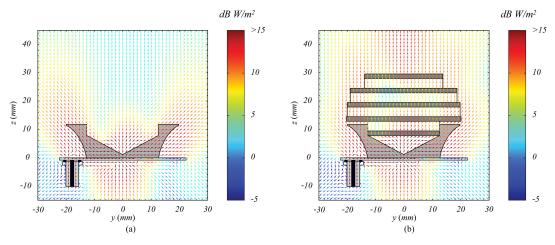
IV. ELECTROMAGNETIC PERFORMANCES OF THE ANTENNA

A prototype of the proposed antenna (shown in Fig. 8) has been manufactured for the experimental verification of the radiative antenna performances. A laser PCB etching machine was used to realized slot, microstrip line, and wide-band radial stub, whereas the horn structure and the dielectric disks forming the lens were made by computer numerical control (CNC) milling. Finally, Pattex® glue by Kleber was used to assemble the horn with the PCB and the dielectric disks with the foam layers used to ensure the desired spacing between the disks. Specific molds were used to accurately assemble the different parts forming the antenna (in Fig. 8 one of the plastic molds used for assembling the horn with the PCB is shown).

The frequency behavior of the input reflection coefficient and realized gain of the final optimized antenna is reported in Fig. 9, while the performance in terms of impedance and axial ratio bandwidth, as predicted numerically and measured on the physical prototype, is detailed in Table 3. As it can

FIGURE 11. Antenna radiation patterns. Working frequencies (a) $f = 8GHz$, (b) $f = 12GHz$. Good agreement with the experimental measurements is observed.

FIGURE 12. Spatial distribution of the real part of the Poynting vector in the yz-plane. Source characteristics: $V_g = 1V$, internal impedance $Z_C = 50\Omega$. Working frequency: 12 GHz. The energy-focusing process due to the 5-stacked-disk dielectric lens and the diffractive processes taking place at the PCB edges are visible in the figure.

be noticed in Table 3, the fractional impedance bandwidth is 92.4% (90% measured), whereas the axial-ratio bandwidth is 67.2% (68% measured). The frequency behavior of the axial ratio is shown in Fig. 10, whereas the LHCP and RHCP gain levels, simulated and measured along the boresight direction ($z - axis$) of the antenna, are reported in Table 4.

Finally, the antenna radiation patterns at the frequencies of 8, and 12 GHz are reported in Fig. 11a and 11b, respectively. A good agreement between numerical simulations and experimental measurements can be observed. The input impedance of the antenna prototype was measured using a Keysight PNA N5225A network analyzer, while the realized gain, the

radiation patterns, and the axial ratio were evaluated using a StarLab multiprobe measurement system available at the facility of The Antenna Company in The Netherlands.

The spatial distribution of the real part of the Poynting vector at the working frequency of 12 GHz is illustrated in Fig. 12. This is useful to gain a better physical insight in the radiation mechanisms underlying the antenna behavior. One can notice the beneficial role played by the stacked-disk lens in focusing the RF energy along the antenna boresight, as well as in reducing the scattered field level by the PCB truncation. Furthermore, the integrated lens significantly increases the axial ratio bandwidth as proved by additional numerical investigations that have not been reported here for brevity.

A performance comparison between the proposed antenna and circularly polarized DRAs already available in the scientific literature is reported in Table 5 (where N.P. stands for "Not Provided" in its reference paper). The table, which highlights the design strategy as well as the CP excitation technique adopted for each considered DRA, shows that, among the antennas with similar fractional bandwidth, the proposed design with shaped horn and lens displays the best performance in terms of gain, axial ratio bandwidth, and compactness.

V. CONCLUSION

A wideband high-gain circularly polarized DHLA operating in the frequency band from 6.7 to 18.2 GHz (FIBW=92.4%), and with an axial ratio smaller than 3 dB between 8.1 and 16.3 GHz (FARBW=67.2%), has been presented. Parametric Lamé equations have been used to describe the optimal geometry of the dielectric horn and lens that ensure the best antenna performance. The adoption of a super-ellipsoidal-axicon dielectric lens has allowed obtaining a peak realized gain of 13.1 dBi, while the use of the S-shaped slot-based excitation scheme has made feasible to excite circular polarization over an extended band of frequencies. Furthermore, it has been demonstrated experimentally for the first time how a stacked-disk dielectric lens can effectively ensure electromagnetic performance similar to that of a massive lens but at a significantly lower cost and weight. The antenna characteristics resulted in good agreement with the measurements carried out on an experimental antenna prototype. The electrical and mechanical features exhibited by the proposed antenna makes it a good candidate in high-gain wideband wireless communication systems as well as in, radar, avionics and satellite applications.

REFERENCES

[1] Y. Zhang, L. Pang, X. Liang, X. Liu, R. Chen, and J. Li, "Propagation characteristics of circularly and linearly polarized electromagnetic waves in urban macrocell scenario," *IEEE Trans. Veh. Technol.*, vol. 64, no. 1, pp. 209–222, Jan. 2015.

[2] B. G. Evans, *Satellite Communication Systems*, 3rd ed. London, U.K.: The Institution of Engineering and Technology, 2008.

[3] I. Nadeem, M. Alibakhshikenari, F. Babaeian, A. A. Althuwayb, B. S. Virdee, L. Azpilicueta, S. Khan, I. Huynen, and F. Falcone, "A comprehensive survey on 'circular polarized antennas' for existing and emerging wireless communication technologies," *J. Phys. D, Appl. Phys.*, vol. 55, no. 3, pp. 1–15, Oct. 2021.

[4] P. Bernardi, R. Cicchetti, and O. Testa, "An accurate UTD model for the analysis of complex indoor radio environments in microwave WLAN systems," *IEEE Trans. Antennas Propag.*, vol. 52, no. 6, pp. 1509–1520, Jun. 2004.

[5] U. Illahi, J. Iqbal, M. I. Sulaiman, M. M. Alam, M. M. Su'ud, and M. H. Jamaluddin, "Singly-fed rectangular dielectric resonator antenna with a wide circular polarization bandwidth and beamwidth for wimax/satellite applications," *IEEE Access*, vol. 7, pp. 66206–66214, 2019.

[6] S. Liu, D. Yang, Y. Chen, S. Huang, and Y. Xiang, "Broadband dual circularly polarized dielectric resonator antenna for ambient electromagnetic energy harvesting," *IEEE Trans. Antennas Propag.*, vol. 68, no. 6, pp. 4961–4966, Jun. 2020.

[7] M. Simeoni, R. Cicchetti, A. Yarovoy, and D. Caratelli, "Plastic-based supershaped dielectric resonator antennas for wide-band applications," *IEEE Trans. Antennas Propag.*, vol. 59, no. 12, pp. 4820–4825, Dec. 2011.

[8] R. Cicchetti, A. Faraone, E. Miozzi, R. Ravanelli, and O. Testa, "A high-gain mushroom-shaped dielectric resonator antenna for wideband wireless applications," *IEEE Trans. Antennas Propag.*, vol. 64, no. 7, pp. 2848–2861, Jul. 2016.

[9] R. Chowdhury, N. Mishra, M. M. Sani, and R. K. Chaudhary, "Analysis of a wideband circularly polarized cylindrical dielectric resonator antenna with broadside radiation coupled with simple microstrip feeding," *IEEE Access*, vol. 5, pp. 19478–19485, 2017.

[10] P. Mallick, M. Ameen, R. Chowdhury, A. K. Ray, and R. K. Chaudhary, "Wideband circularly polarized cavity-backed dielectric resonator antenna with low RCS for aerial vehicle communications," *IEEE Antennas Wireless Propag. Lett.*, vol. 21, no. 7, pp. 1418–1422, Jul. 2022.

[11] M. Zou, J. Pan, Z. Nie, and P. Li, "A wideband circularly polarized rectangular dielectric resonator antenna excited by a lumped resistively loaded monofilar-spiral-slot," *IEEE Antennas Wireless Propag. Lett.*, vol. 12, pp. 1646–1649, 2013.

[12] M. Zou, J. Pan, and Z. Nie, "A wideband circularly polarized rectangular dielectric resonator antenna excited by an Archimedean spiral slot," *IEEE Antennas Wireless Propag. Lett.*, vol. 14, pp. 446–449, 2015.

[13] H. N. Chen, J.-M. Song, and J.-D. Park, "A compact circularly polarized MIMO dielectric resonator antenna over electromagnetic band-gap surface for 5G applications," *IEEE Access*, vol. 7, pp. 140889–140898, 2019.

[14] X. S. Fang, L. P. Weng, and Y.-X. Sun, "Slots-coupled omnidirectional circularly polarized cylindrical glass dielectric resonator antenna for 5.8-GHz WLAN application," *IEEE Access*, vol. 8, pp. 204718–204727, 2020.

[15] N. Yang, K. W. Leung, K. Lu, and N. Wu, "Omnidirectional circularly polarized dielectric resonator antenna with logarithmic spiral slots in the ground," *IEEE Trans. Antennas Propag.*, vol. 65, no. 2, pp. 839–844, Feb. 2017.

[16] F.-R. Hsiao, T.-W. Chiou, and K.-L. Wong, "Circularly polarized low-profile square dielectric resonator antenna with a loading patch," *Microw. Opt. Technol. Lett.*, vol. 31, no. 3, pp. 157–159, Nov. 2001.

[17] K. W. Leung, W. C. Wong, and H. K. Ng, "Circularly polarized slot-coupled dielectric resonator antenna with a parasitic patch," *IEEE Antennas Wireless Propag. Lett.*, vol. 1, pp. 57–59, 2002.

[18] K. X. Wang and H. Wong, "A circularly polarized antenna by using rotated-stair dielectric resonator," *IEEE Antennas Wireless Propag. Lett.*, vol. 14, pp. 787–790, 2015.

[19] W.-W. Yang, W.-J. Sun, H. Tang, and J.-X. Chen, "Design of a circularly polarized dielectric resonator antenna with wide bandwidth and low axial ratio values," *IEEE Trans. Antennas Propag.*, vol. 67, no. 3, pp. 1963–1968, Mar. 2019.

[20] S. Hossain, "5G wireless communication systems," *Amer. J. Eng. Res.*, vol. 2, no. 10, pp. 344–353, 2013.

[21] R. Cicchetti, E. Miozzi, and O. Testa, "Wideband and UWB antennas for wireless applications: A comprehensive review," *Int. J. Antennas Propag.*, vol. 2017, pp. 1–45, Feb. 2017.

[22] S. K. K. Dash, T. Khan, and Y. M. M. Antar, "A state-of-art review on performance improvement of dielectric resonator antennas," *Int. J. RF Microw. Comput.-Aided Eng.*, vol. 28, no. 6, Aug. 2018, Art. no. e21270.

[23] M. Gardner, *The Colossal Book of Mathematics*. New York, NY, USA: Norton, 2001.

[24] R. Cicchetti, V. Cicchetti, A. Faraone, and O. Testa, "A class of lightweight spherical-axicon dielectric lenses for high gain wideband antennas," *IEEE Access*, vol. 9, pp. 151873–151887, 2021.

[25] R. K. Mongia and P. Bhartia, "Dielectric resonator antennas—A review and general design relations for resonant frequency and bandwidth," *Int. J. Microw. Millim.-Wave Comput.-Aided Eng.*, vol. 4, no. 3, pp. 230–247, Jul. 1994.

[26] A. A. Kishk, Y. Yan, and A. W. Glisson, "Conical dielectric resonator antennas for wide-band applications," *IEEE Trans. Antennas Propag.*, vol. 50, no. 4, pp. 469–474, Apr. 2002.

[27] R. Cicchetti, V. Cicchetti, A. Faraone, L. Foged, and O. Testa, "A wideband high-gain dielectric horn-lens antenna for wireless communications and UWB applications," *IEEE Trans. Antennas Propag.*, vol. 71, no. 2, pp. 1304–1318, Feb. 2023.

[28] L. Mescia, P. Bia, D. Caratelli, M. A. Chiapperino, O. Stukach, and J. Gielis, "Electromagnetic mathematical modeling of 3D supershaped dielectric lens antennas," *Math. Problems Eng.*, vol. 2016, pp. 1–10, Jan. 2016, doi: 10.1155/2016/8130160.

DIEGO CARATELLI (Senior Member, IEEE) was born in Latina, Italy, in 1975. He received the M.Sc. degree (summa cum laude) in applied mathematics and the Laurea (summa cum laude) and Ph.D. degrees in electronic engineering from the Sapienza University of Rome, Rome, Italy, in 2000, 2004, and 2013, respectively. He received the MicroMaster in principles of manufacturing from the Massachusetts Institute of Technology, Cambridge, MA, USA, in 2022.

From 2005 to 2007, he was a Research Fellow with the Department of Electronic Engineering, Sapienza University of Rome. From 2007 to 2013, he was a Senior Researcher with the International Research Center for Telecommunications and Radar, Delft University of Technology, Delft, The Netherlands. From 2015 to 2019, he was an Associate Professor with the Institute of Cybernetics, Tomsk Polytechnic University, Tomsk, Russia. In 2013, he has co-founded The Antenna Company, Eindhoven, The Netherlands, where he is currently the Chief Technology Officer/the Vice-President of engineering, where he is responsible for product development, program portfolio management, and technical direction of the research and development team. Since 2020, he has been an Associate Professor with the Group of Electromagnetics in Wireless Telecommunications, Eindhoven University of Technology, Eindhoven. He has authored or coauthored more than 225 publications in international peer-reviewed journals, book chapters, and conference proceedings. He holds 27 families of patents in antenna-related technologies and advanced computational techniques. His current research interests include full-wave analysis, design of passive devices, and antennas for satellite, wireless, and radar applications, the development of analytically based numerical techniques devoted to the modeling of wave propagation and diffraction processes, the theory of special functions for electromagnetics, the deterministic synthesis of sparse antenna arrays, and the solution of boundary-value problems for partial differential equations of mathematical physics.

Dr. Caratelli has been a member of the IEEE Technical Committee TC-34 on Nanotechnology in Instrumentation and Measurement of the IEEE Instrumentation and Measurement Society, since 2014. He is currently a member of the Applied Computational Electromagnetics Society (ACES), the Institution of Engineering and Technology (IET), the International Union of Radio Science (URSI), and the Italian Electromagnetic Society (SIEm). He was a recipient of the Young Antenna Engineer Prize at the 32nd European Space Agency Antenna Workshop and the 2010 Best Paper Award from ACES. He was a co-recipient of the Frost and Sullivan Best Practices Award for technology innovation in advanced antennas for wireless communications in 2016. He is the Lead Guest Editor of the Special Issue on Antenna Array Design for Wireless Communications and Remote Sensing of MDPI *Sensors* and the Special Issue on Theory and Applications of Special Functions in Mathematical Physics of MDPI *Symmetry*.

RENATO CICCHETTI (Life Senior Member, IEEE) was born in Rieti, Italy, in 1957. He received the Laurea degree (summa cum laude) in electronics engineering from the University of Rome "La Sapienza," Rome, Italy, in 1983. From 1983 to 1986, he was an Antenna Designer with Selenia Spazio S.p.A. (currently Thales Alenia Space S.p.A.), Rome, where he was involved in studies on theoretical and practical aspects of antennas for space application and scattering problems. From 1986 to 1994, he was a Researcher, and from 1994 to 1998, he was an Assistant Professor with the Department of Electronics Engineering, University of Rome "La Sapienza," where he is currently a Full Professor. In 1998, 2002, and 2006, he was a Visiting Professor with the Motorola Florida Corporate Electromagnetics Research Laboratory, Fort Lauderdale, FL, USA, where he was involved in antennas for cellular and wireless communications. From 2017 to 2021, he was one of the coordinators of the research project "Ultra-Wideband Virtual Imaging Extra Wall for High-Penetration High Quality Imagery of Enclosed Structures" (U-VIEW) funded by the Italian Ministry of Education, University and Research (MIUR). His current research interests include electromagnetic field theory, asymptotic techniques, electromagnetic compatibility, wireless communications, microwave and millimeter-wave integrated circuits, and antennas. He is a member of the Italian Electromagnetic Society (SIEm) and his results listed in Marquis Who's Who in the World and Who's Who in Science and Engineering. Since 2012, he has been the Lead Editor of the annual Special Issue on Wideband, Multiband, Tunable, and Smart Antenna Systems for Mobile and UWB Wireless Applications for the *International Journal of Antennas and Propagation*.

VALENTINA CICCHETTI was born in Isernia, Italy, in 1993. She received the master's degree (cum laude) in electronic engineering and the Ph.D. degree from the University of Rome "La Sapienza," Rome, Italy, in 2018 and 2022, respectively. Her research interests include applied electromagnetics, wideband and ultra-wideband antenna systems, and the analysis of the related electromagnetic compatibility problems.

ORLANDINO TESTA received the Laurea degree (cum laude) in electronic engineering and the Ph.D. degree from the University of Rome "La Sapienza," Rome, Italy, in 1997 and 2003, respectively. Since 2001, he has been a high school Teacher with the ITIS "G. Armellini" Institute of Rome, Rome, where he is involved in teaching electronics and telecommunications. He is currently collaborating with the Department of Electronic Engineering, University of Rome "La Sapienza." He is also studying high-frequency models for near- and far-field synthesis, design of dielectric resonator antennas (DRAs) equipped with lens for communication and through-the-wall imaging (TWI) applications. His research interests include propagation and radiation of electromagnetic fields, electromagnetic compatibility, microwave and millimeter-wave integrated circuits, and antennas.

• • •